ACS OMEGA

http://pubs.acs.org/journal/acsodf

Article

Preparation of a Superhydrophobic Surface by a One-Step Powder Pressing Method with Liquid Silicone Rubber As the Carrier

Zhen Wei, Fangyuan Zhang, Fei Dai,* and Qiang He*

Cite This: *ACS Omega* 2023, 8, 8548−8556

Read Online

ACCESS | Metrics & More | Article Recommendations

ABSTRACT: The preparation methods of the superhydrophobic surface play an important role in its application, but most of the existing preparation methods are complicated in operation, high in cost, and polluting to the environment. In order to find a simple, rapid, low-cost, and nonenvironmentally polluting preparation method of the superhydrophobic surface, this paper used liquid silicone rubber as the carrier. Before the liquid silicone rubber was nearly cured, it was evenly covered with a layer of silicon dioxide powder, and then 5 N weight was used to compact the powder on the rubber surface, so that the superhydrophobic surface was quickly formed on its surface. The wettability, bouncing performance, self-cleaning performance, and bending durability of liquid silicone rubber before and after treatment were compared. The results show that the static contact angle and rolling angle of the liquid silicone rubber after powder pressing were 158.22 ± 2.01° and 1.00 ± 0.50°, respectively. Moreover, the superhydrophobic surface formed by the powder pressing method had good self-cleaning performance, high temperature resistance, bending resistance, and excellent droplet bounce performance. The strategy of preparing a superhydrophobic surface by a one-step powder pressing method may be applied to the preparation of the superhydrophobic surface on a large scale.

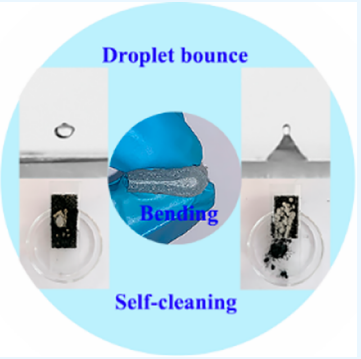

1. INTRODUCTION

Superhydrophobic surface refers to the surface where the contact angle between water droplets and solid materials is greater than 150°, and the rolling angle is less than 10° when solid materials are in contact with water droplets.[1−5] Superhydrophobic surfaces are widely used in industry, military, and daily life because of their excellent hydrophobicity.[6−9] An important application of superhydrophobic surfaces is self-cleaning,[10] which can effectively improve the waterproof and antifouling ability of its surface when it is used on glass, clothing, and metal. Superhydrophobic materials can also be used in pipeline antiscaling, oil−water separation, drag reduction, antiskid, anticorrosion, and other applications. Therefore, the research and development of superhydrophobic materials is of great significance to daily life and industrial development. The current method of forming a superhydrophobic surface is to construct a micronano structure on the surface with low surface energy or modify the micronano structure with low surface energy substances.[11−14] At present, the methods for preparing superhydrophobic surfaces mainly include: the layer-by-layer self-assembly method,[15] spraying method,[16] template method,[17] chemical vapor deposition method,[18] sol−gel method,[19] etching method,[20] spin-coating method,[21] and so on. For example, Chi[22] and others used hydrophobic silicon dioxide particles and organosilane binder to prepare an antireflection coating with mechanical firmness and self-cleaning performance. Wang[23] et al. used traditional nucleophilic polycondensation and simple electrospray technology to modify common polyaryletherketone (PAEK) into hexafluorobisphenol A-PAEK and prepared a new superhydrophobic polyaryletherketone membrane for the first time. He[24] et al. prepared a three-dimensional superoleophilic/superhydrophobic carbon fiber felt (CFF) material surface by anchoring hydrophobic Fe_3O_4 nanoparticles on 3D CFF. The prepared CFF material showed high water contact angle and low oil contact angle. Davis[25] et al. produced a highly solid superhydrophobic silicone whole through expandable and environmentally friendly emulsion technology. It is first found that stable and surfactantless water-in-polydimethylsiloxane (PDMS) emulsions can be formed through mechanical mixing, and they had good durability. Bayer[26] et al. mentioned that perfluorinated compounds can cause some environmental problems. Moreover, most of the formulations and processes of superhydrophobic coatings were considered to be not environmentally friendly, unable to maintain large-scale manufacturing, or too expensive to be converted into a standard industrial practice. Recently, however, people had made superhydrophobic coatings by using natural materials and

Received: December 2, 2022
Accepted: February 13, 2023
Published: February 23, 2023

https://doi.org/10.1021/acsomega.2c07241
ACS Omega 2023, 8, 8548−8556

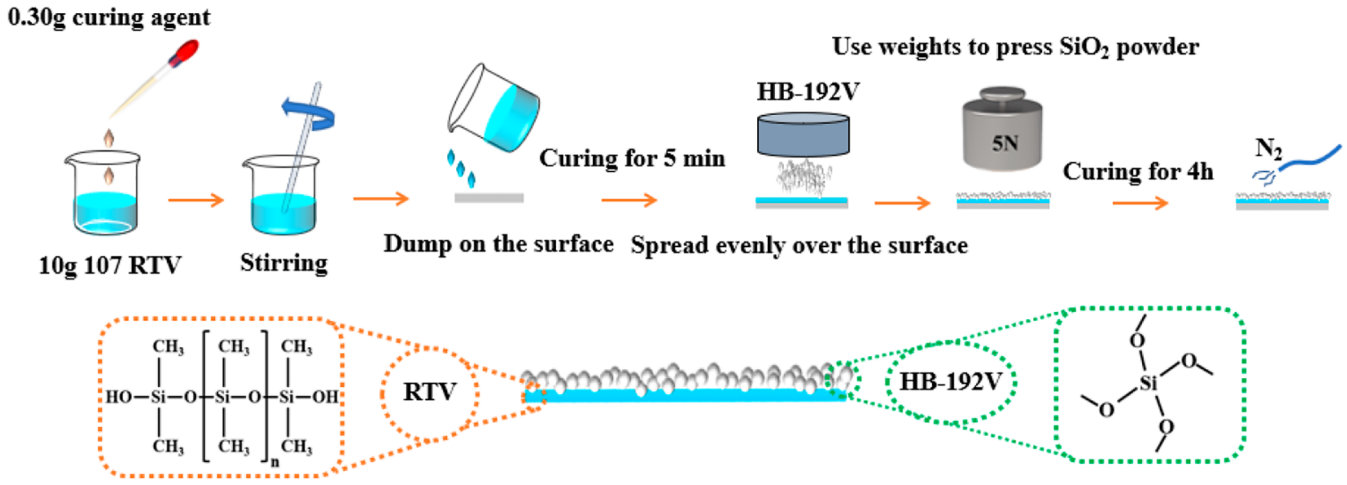

Figure 1. Flowchart of the sample preparation process.

sustainable processes, thus reducing potential environmental pollution.

Silicone rubber is widely used in antifouling coatings, aerospace, machinery, biomedicine, electrical insulators, and other fields because of its superior weather resistance, electrical insulation, transparency, low toxicity, and hydrophobicity.[27−29] Therefore, silicone rubber is favored by many scholars in the preparation of superhydrophobic surfaces.[30,31] For example, Maghsoudi[32] et al. directly copied the surface of superhydrophobic high-temperature vulcanized silicone rubber by a compression molding system, and its surface contact angle was greater than 160° and rolling angle less than 3°. Wan[33] et al. put forward a simple and cheap dipping−coating−curing strategy. A strong, environmentally friendly melamine-formaldehyde sponge with a superhydrophobic and superoleophilic MoS_2 coating was prepared through the modification of room-temperature vulcanized silicone rubber. Most of the preparation methods of superhydrophobic surfaces have limitations. For example, although the spraying method is simple in operation and low in cost, it emits pollution to the environment. Also, the etching process is complicated; the cost is high; and it is not suitable for mass production.

In this work, the liquid silicone rubber was used as the carrier, and before the liquid silicone rubber was nearly cured, a layer of silicon dioxide powder was evenly covered on its surface. Then the powder on the rubber surface was compacted with a 5 N weight, so that its surface quickly formed a superhydrophobic surface. In order to test the performance of the superhydrophobic surface, self-cleaning, high-temperature resistance, bending durability, and droplet bounce performance were tested.

2. EXPERIMENTAL

2.1. Materials. Silicon dioxide (HB-192V) was purchased from Yichang Huifu Silicon Materials Co., Ltd., Hubei Province (China). Liquid silicone rubber (RTV, 107−1705) and curing agents were purchased from Shandong Heyuan Chemical Co., Ltd. (China). Fluorosilicone rubber (FVMQ, FSR8460-U) was purchased from Dongguan Ningdao Rubber Industry Co., Ltd. (China). 2,5-Dimethyl-2,5-di(*tert*-butylperoxy)hexane (DBPH), the curing agent, was purchased from Zijun Chemical Co., Ltd. (China). A release agent and polydimethylsiloxane aqueous emulsion were purchased from Jiahong Technology (China). Anhydrous ethanol was purchased from Fuyu Chemical Co., Ltd. (China). Carbon black was purchased from Jiangsu Jiujia Biotechnology Co., Ltd.

2.2. Sample Preparation. In this work, FVMQ was used as the substrate (the actual situation of the substrate can be any solid). First, FVMQ was polished on a metallographic sample polishing machine to make its surface rough, and then FVMQ was washed in an ultrasonic box with absolute ethanol for 10 min. Finally, we took it out and dried it in a blast drying oven. An amount of 10.00 g of RTV was weighed by an electronic analytical balance, and 0.30 g of curing agent (the curing agent was 3% of silicone rubber) was mixed in a beaker and stirred for 3 min with a glass rod to obtain a mixed solution, and then we evenly coated the mixed solution on the FVMQ surface cleaned with absolute ethanol and cured the RTV at room temperature for 5−8 min. Second, HB-192V powder was evenly scattered on the surface of the incompletely cured RTV through a 200-mesh screen to obtain an RTV/HB-192V sample with a layer of HB-192V particles uniformly covered on the surface layer. After standing for 1 h, HB-192V particles covered on RTV were compacted with a 5 N weight, so that HB-192V particles were closely combined with RTV. Then, RTV/HB-192V samples were naturally cured at room temperature for 4 h. After curing, HB-192V powder not adhered to the rubber surface was cleaned with nitrogen. The process flowchart of the RTV/HB-192V sample preparation is shown in Figure 1.

2.3. Performance Test and Characterization. Using a contact angle tester (HKCA-15, Beijing Hake Test Instrument Factory (China)), five points were randomly selected for the static contact angle test (the volume of the liquid was 4.00 μL) on two kinds of rubber surfaces, and the sliding angle of two kinds of rubber surfaces was measured by 15.00 μL droplets.

Carbon black was used to simulate dust, which was evenly sprinkled on the surfaces of two kinds of rubber. The RTV/HB-192V sample was placed in a culture dish with a diameter of 60.00 mm and an inclination angle of 26.60° with a glass slide as a carrier. Water droplets (with a volume of 5.00 μL) dropped from 10 mm at the higher end of the two kinds of rubber surfaces through a rubber dropper, and the behavior of the droplets rolling on different rubber surfaces to take away the dust was observed. With a high-speed camera (HX-6E, MEMRECAM Company (Japan)), the bouncing test of water droplets with sizes of 5.00 and 10.00 μL was carried out on two kinds of rubber

https://doi.org/10.1021/acsomega.2c07241
ACS Omega 2023, 8, 8548−8556

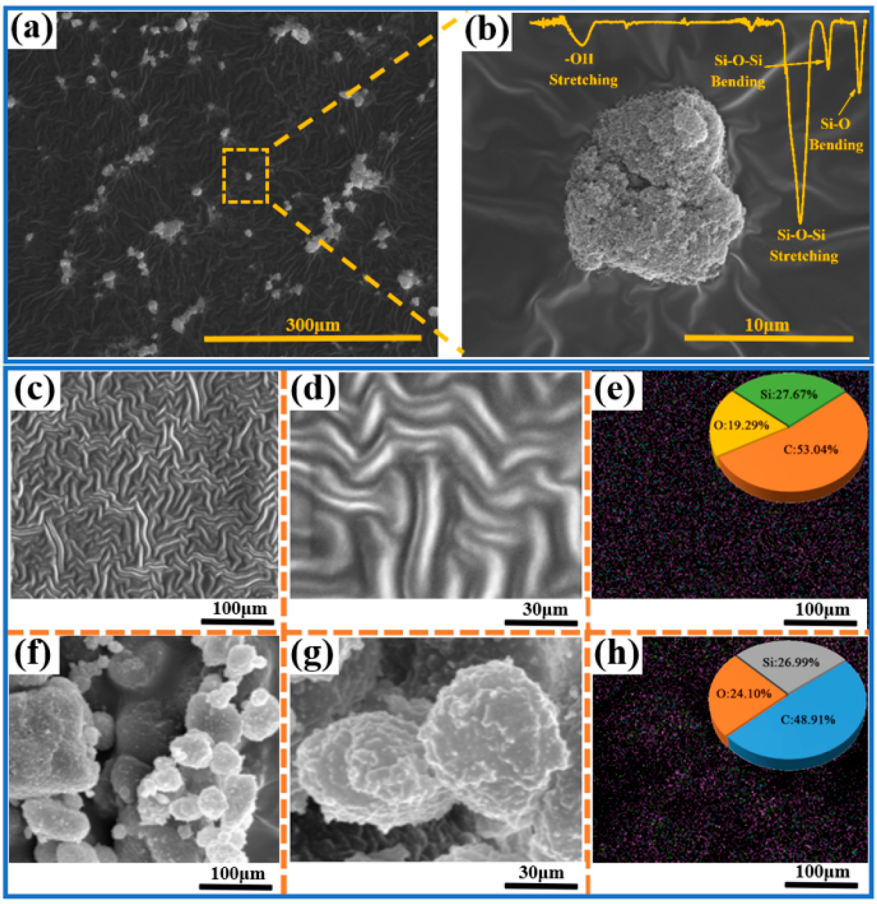

Figure 2. SEM of HB-192V in alcohol solution (a). HB-192V particles and FTIR (b). SEM of the RTV surface (c). Enlarged electron microscope image of the RTV surface (d). Element distribution and element content percentage on the RTV surface (e). SEM of RTV/HB-192V (f). Local magnified electron microscope image of RTV/HB-192V (g). Element distribution and element content percentage on the RTV/HB-192V surface (h).

surfaces from four different heights, and the bouncing of water droplets on RTV and RTV/HB-192V surfaces was compared and analyzed.

The RTV/HB-192V sample was subjected to a 72 h high-temperature aging test by a hot air aging tester (MU3040C, Shanghai Moujing Industrial Co., Ltd.), and the aging temperature was set at 150.00 °C. The influence of high-temperature aging on the superhydrophobic surface was analyzed. A Fourier transform infrared spectrometer (FTIR, IRTracer-100, Shimadzu, Japan) was used to compare and analyze the changes of superhydrophobic surface functional groups of HB-192V particles and RTV/HB-192V samples before and after high-temperature aging. The bending durability of the RTV/HB-192V sample was tested by 500 bending tests, and the influence of the bending durability test on the superhydrophobic surface was analyzed.

A metallographic sample polishing machine (PG-1, Shenyouda Industrial Co., Ltd. (China)) was used to polish the FVMQ substrate surface. An ultrasonic box (500DE, Kunshan Ultrasonic Instrument Co., Ltd.) was used to wash the FVMQ matrix. We dried the sample by a blast drying oven (9070A, Shanghai Heng Science Instrument Co., Ltd. (China)). A weight (Shandong Penglai Shuiling Weight Factory, China) was used to compact the silica powder adsorbed on the surface of liquid silicone rubber. Then, the microstructures of the RTV surface and the RTV/HB-192V surface were observed by a scanning electron microscope (SEM450, NOVANANO Company (USA)) and three-dimensional topography instrument (ST-400M, NANOVEA Company (USA)), and the element distribution of the two rubber surfaces was observed by an energy-dispersive spectrometer (EDS).

3. RESULTS AND DISCUSSION

3.1. Surface Morphology and Hydrophobic Properties. It can be seen from Figure 2(a) that HB-192V particles in the solution were agglomerated after ultrasonic dispersion with alcohol solution. It can be seen from Figure 2(b) that the HB-192V particles were spherical in appearance, with a diameter of about 11 μm. When the particles were adsorbed on the rubber surface, the convex structure of the rubber surface was increased, and the main characteristic peaks of the particles are −OH, Si−O−Si, stretching vibration, and bending vibration of Si−O bonds.

It can be seen from Figure 2(c−e) that the surface of RTV was smooth and had a grain structure. According to the element distribution and element proportion on the RTV surface, three elements, C, O, and Si, were uniformly distributed on the RTV surface, among which the element content of Si was 27.67%; that of O was 19.29%; and that of C was 53.04%. It can be seen from Figure 2(f) that HB-192V powder was successfully attached to the surface of RTV. It can be seen from Figure 2(f) and Figure 2(g) that there was a gap between HB-192V particles attached to the rubber surface, and there was local agglomeration. This phenomenon will cause the exposed HB-192V particles and air

https://doi.org/10.1021/acsomega.2c07241
ACS Omega 2023, 8, 8548−8556

molecules to establish a Cassie−Baxter model[34] in the microstructure. According to the surface element distribution and element proportion of RTV/HB-192V in Figure 2(h), the content of element C was 48.91%, and that of O was 24.10%. According to Figure 2(e) and Figure 2(h), the formula element ratio of silicon dioxide was Si:O = 1:2. It can be seen that the content of the silicon element decreases, and the content of elemental oxygen increases on the rubber surface after pressing HB-192V, which proves that HB-192V powder successfully adheres to the RTV surface.

According to the three-dimensional topography of the rubber surface in Figure 3(a), the surface of RTV was smooth, and the

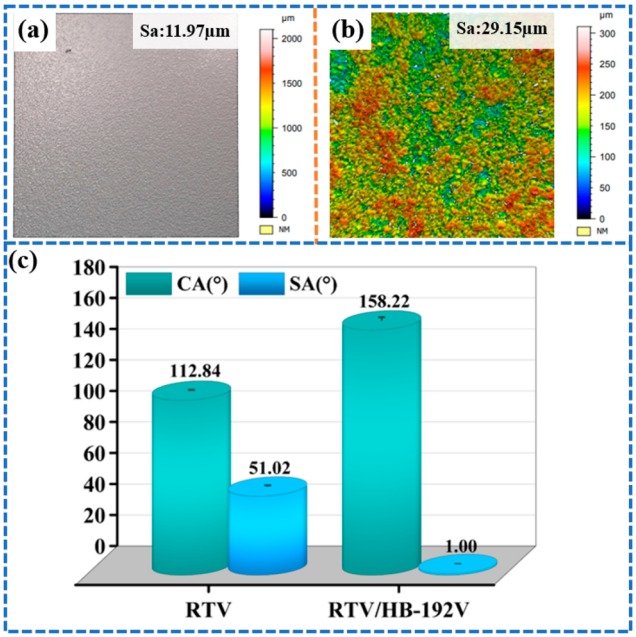

Figure 3. Three-dimensional topography of the RTV surface (a). Three-dimensional topography of the RTV/HB-192V surface (b). Comparative histogram of the static contact angle and rolling angle of the RTV surface and RTV/HB-192V surface (c).

microscopic condition of the rubber surface shown in Figure 2(c) was verified. The surface roughness (Sa) of RTV was 11.97 μm. After the surface of RTV was covered with HB-192V particles, the Sa on the surface of RTV was increased to 29.15 μm, which was 1.44 times that of the surface without powder pressing. Therefore, the powder pressing behavior increased the surface roughness of RTV, and a layer of microstructure covered by HB-192V particles was formed on the surface of RTV.

According to Figure 3(c), the average contact angle and rolling angle of the RTV surface were 112.84° and 51.02°, and the average contact angle and rolling angle of the RTV/HB-192V surface were 158.22° and 1.00°, respectively. Because the contact angle of the RTV surface was greater than 90.00°, its surface was hydrophobic. After coating a layer of HB-192V powder on the RTV surface, HB-192V particles form a microstructure on the RTV surface, which increased the roughness of the rubber surface, which greatly improved the hydrophobic property of the RTV/HB-192V surface. The rolling angle of the RTV surface was 51.02 ± 0.78°, which indicated that the droplet adhesion of the RTV surface was relatively large, which led to the larger rolling angle of the RTV surface. The rolling angle of the RTV/HB-192V surface measured by a contact angle tester was 1.00 ± 0.50°, which proved that the RTV surface covered by HB-192V powder showed good superhydrophobic performance.

3.2. Droplet Bounce Performance Test. It can be seen from Figure 4(a) and Figure 4(e) that water droplets of the same volume lag behind at different heights, and with the increase of drop height, the spreading diameter of the droplets on the surface of RTV/HB-192V gradually increased. It takes longer to reach the maximum spreading diameter. This was because the higher the drop height, the greater the gravitational potential energy of the droplets when the droplets touched the surface of RTV/HB-192V. The gravitational potential energy and kinetic energy of the drop were converted into the surface energy of the drop. The higher the drop falling distance, the larger the surface energy and the larger the surface area of the drop. Therefore, when the drop fell at different heights, the larger the height, the larger the surface area, and the larger the spreading diameter of the drop. According to the comparison of Figure 4(a), Figure 4(b), and Figure 4(e), when different volumes of droplets fall at the same height, the larger the volume of droplets, the larger the maximum spreading diameter of droplets on the surface of RTV/HB-192V. This was because the larger the volume of the droplets, the larger the diameter of the droplets; therefore, when droplets with different volumes at the same height fell on the surface of RTV/HB-192V, the largest spreading diameter of droplets with larger volume will be larger.

It can be seen from Figure 4(c) and Figure 4(f) that the droplets with the same volume fell behind at different heights, and with the increase of the falling height of the droplets, the maximum bounce height of the droplets after contacting the rubber surface was larger. The time to reach the maximum bounce height was longer. The reason was that the higher the drop height, the greater the gravitational potential energy of the drop. Because the surface of RTV/HB-192V had a microstructure, the gravitational potential energy and kinetic energy of the drop were converted into the surface energy of the drop, and a part of the potential energy was lost by impact and then converted into gravitational potential energy and kinetic energy. The more gravitational potential energy was converted, the higher the maximum bounce height of the drop. According to the comparison of Figure 4(c) and Figure 4(d), when the droplets with different volumes fell on the surface of RTV/HB-192V at the same height, the larger the droplet volume, the smaller the maximum bouncing height of the droplets. The analysis may be that when the droplets with larger volume fell on the surface of RTV/HB-192V at the same height, the larger the droplet volume, the larger the maximum spreading diameter. The larger the contact area, the more energy will be lost to overcome the friction resistance provided by the contact layer when the droplets bounce. Therefore, when droplets with different volumes at the same height drop, the maximum bounce height of droplets with small volume was larger.

It can be seen from Figure 4(g) that when water drops on the surface of RTV the water drops did not rebound but repeatedly stretched and shrank on the surface of RTV and then stopped steadily, indicating that there were strong water drops attached on the surface of RTV.

3.3. Self-Cleaning Test. It can be seen from Figure 5(a) that when 5 drops of water were dropped on the surface of RTV the drops were clustered together and adsorbed on the surface of RTV. As the water drops increased to 15 drops, all the drops still clustered together and did not roll down the slope. It can be seen from Figure 5(b) that when five drops of water drop at the same

https://doi.org/10.1021/acsomega.2c07241
ACS Omega 2023, 8, 8548−8556

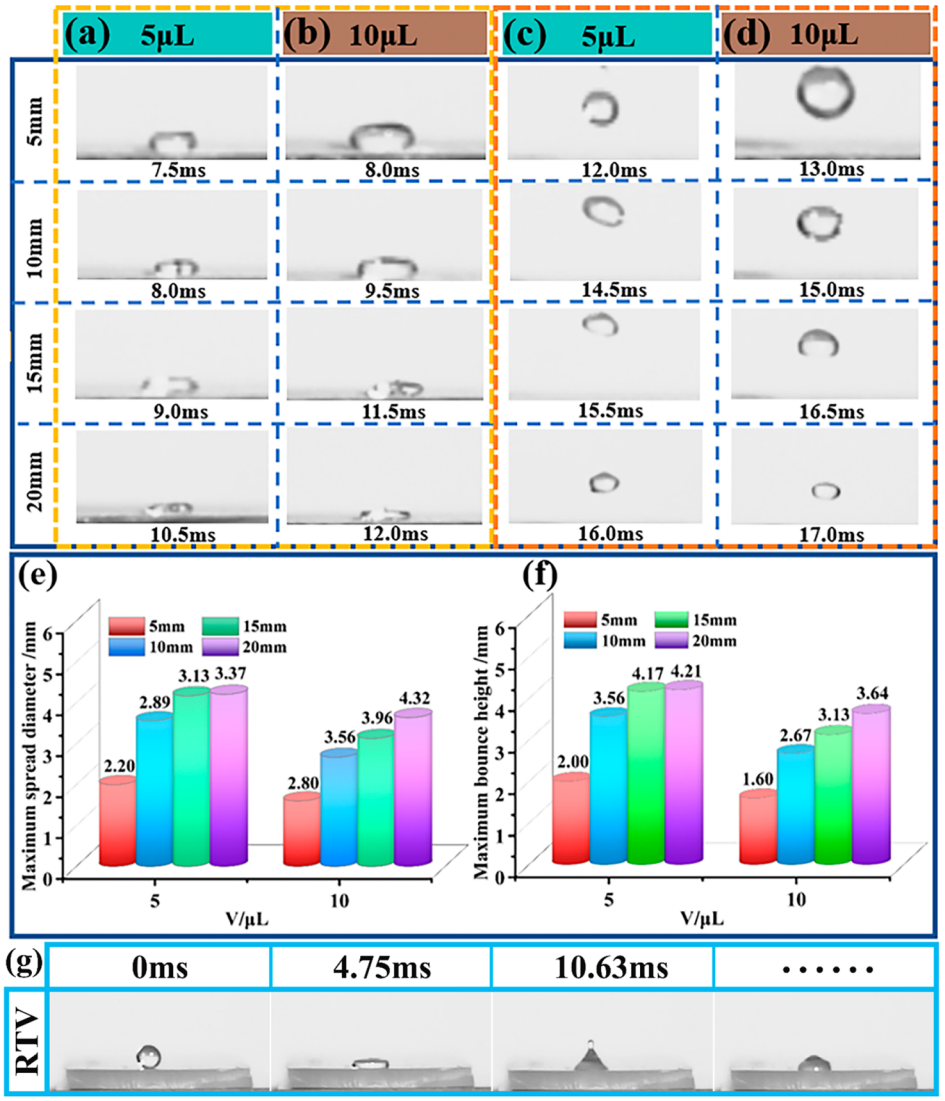

Figure 4. Spreading behavior of droplets with different volumes falling on the surface of RTV/HB-192V at different heights (a,b). The bouncing behavior of droplets with different volumes falling on the surface of RTV/HB-192V at different heights (c,d). Maximum spreading diameter of droplets with different volumes falling from different heights to the surface of RTV/HB-192V (e). Droplets of different volumes fall from different heights to the maximum bouncing height of the RTV/HB-192V surface (f) and droplet bounce behavior of droplets dropping from 15 mm height to the RTV surface (g).

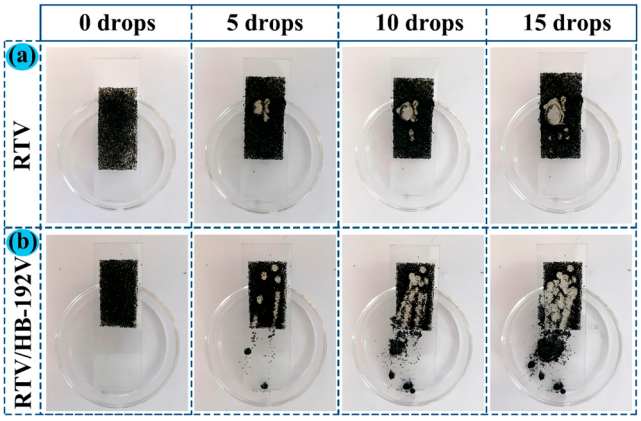

Figure 5. Self-cleaning experimental process of original silicone rubber (a) and self-cleaning experimental process of silicone rubber composites (b).

height on the surface of the RTV/HB-192V sample some drops bounced and rolled down quickly with carbon black. When the number of water drops increased to 15 drops, most of the carbon black on the surface of RTV/HB-192V had been taken away by water drops, and an obvious channel was formed on the rubber surface. Through the comparison of two groups of self-cleaning test phenomena, it can be seen that the RTV surface treated by HB-192V powder had a good self-cleaning effect.

3.4. Durability Test. It can be seen from Figure 6(a) and Figure 6(b) that the Sa of the RTV surface was 11.97 μm. After 72 h of high-temperature aging, the Sa of the RTV surface was increased to 37.91 μm. The high-temperature aging test increased the roughness of the RTV surface. It can be seen from Figures 6(c) and 6(d) that the Sa of the RTV/HB-192V surface was 29.15 μm, which was larger than the surface roughness of RTV. After high-temperature aging, the Sa of the RTV/HB-192V surface was 45.93 μm, compared with that before aging. The surface roughness was increased, and the

https://doi.org/10.1021/acsomega.2c07241
ACS Omega 2023, 8, 8548−8556

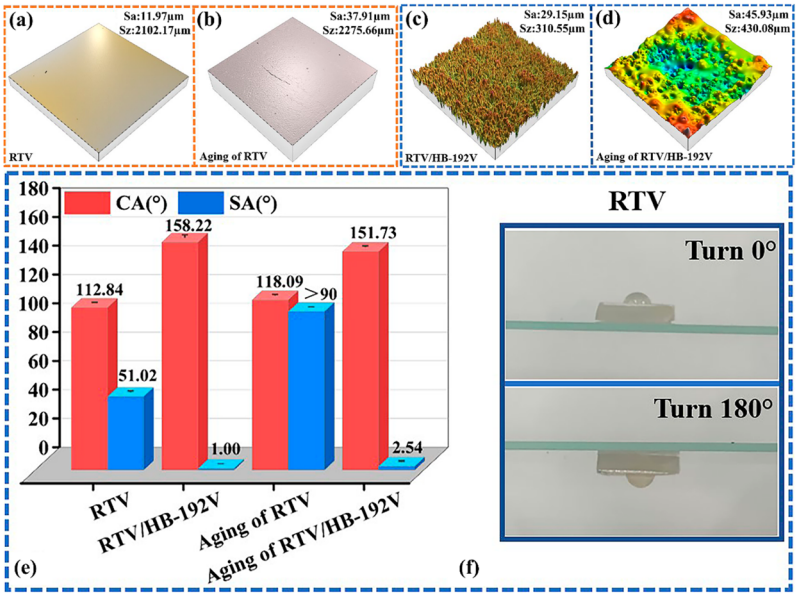

Figure 6. Comparison of three-dimensional morphology of RTV and RTV/HB-192V surfaces before and after high-temperature aging (a–d). Comparison of the contact angle and rolling angle of RTV and RTV/HB-192V surfaces before and after high-temperature aging (e). Supplementary test chart of the rolling angle of RTV after high-temperature aging (f).

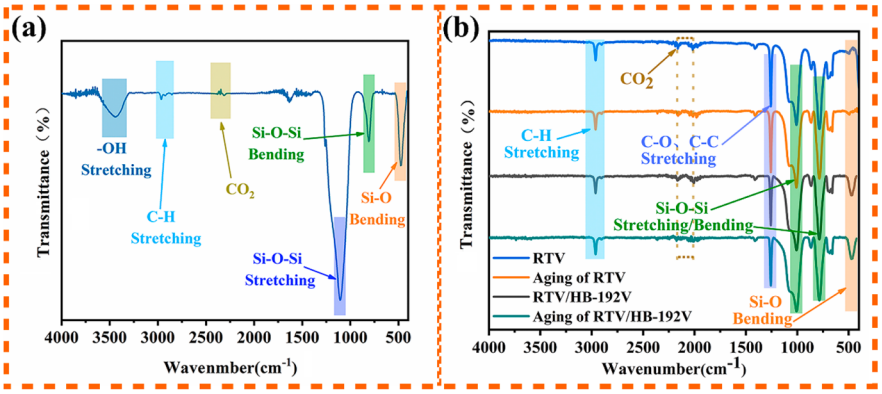

Figure 7. Fourier infrared spectrum of HB-192V particles (a). Comparison of FTIR spectra of RTV and RTV/HB-192V before and after high-temperature aging (b).

change trend of Sa was the same as that before and after aging of RTV. By comparison, the maximum height of RTV and the RTV/HB-192V surface before and after high-temperature aging was increased, which proves that it was raised in the *Z* direction, which increased the surface roughness.

According to Figure 6(e), the contact angle of the RTV surface was 112.84 ± 0.55°; the rolling angle was 51.02 ± 0.78°; the contact angle of the RTV/HB-192V surface was 158.22 ± 2.01°; and the rolling angle was 1.00 ± 0.50°. After 72 h of high-temperature aging, the contact angle of the RTV surface becomes 118.09 ± 0.76°, which was 5.25° larger than that before aging, indicating that the increase of surface roughness increases the contact angle after high-temperature aging. Figure 6(f) shows the phenomenon that water droplets fell on the surface of RTV after aging and rotated 180°, but the droplets still did not fall, indicating that the rolling angle of the RTV surface after high-temperature aging was greater than 90° and had strong adsorption. After aging, the contact angle of the RTV/HB-192V surface was 151.73 ± 0.86°, which was 6.49° lower than that before aging. After aging, the rolling angle was 2.54 ± 0.62°, which was 1.54° higher than that before aging at high temperature. The reason was that as the roughness of the surface increases the air cavity between concave and convex structures becomes larger, and the air density in a certain space decreases. The results show that the surface of RTV/HB-192V was still superhydrophobic after 72 h of a high-temperature aging test, which indicated that this superhydrophobic surface had good high-temperature durability.

It can be seen from Figure 7(a) and Figure 7(b) that the characteristic peak at 3445 cm^{-1} was the tensile vibration peak of hydroxyl (−OH) in water molecules. The characteristic peaks at 1100 cm^{-1} and 810 cm^{-1} were caused by the tensile vibration and bending vibration of the Si−O−Si bond, and the characteristic peak at 2965 cm^{-1} was the tensile vibration peak of the C−H bond. The characteristic peak at 2345 cm^{-1} was produced by carbon dioxide. After RTV was covered with HB-192V powder, C−O and C−C on the surface of RTV could still be detected, while the water hydroxyl groups in the particles disappeared. It was speculated that the particles were adsorbed on the RTV surface and dried for a long time, so the water hydroxyl group was removed. According to the peak comparison between the two rubbers before and after high-temperature

https://doi.org/10.1021/acsomega.2c07241
ACS Omega 2023, 8, 8548−8556

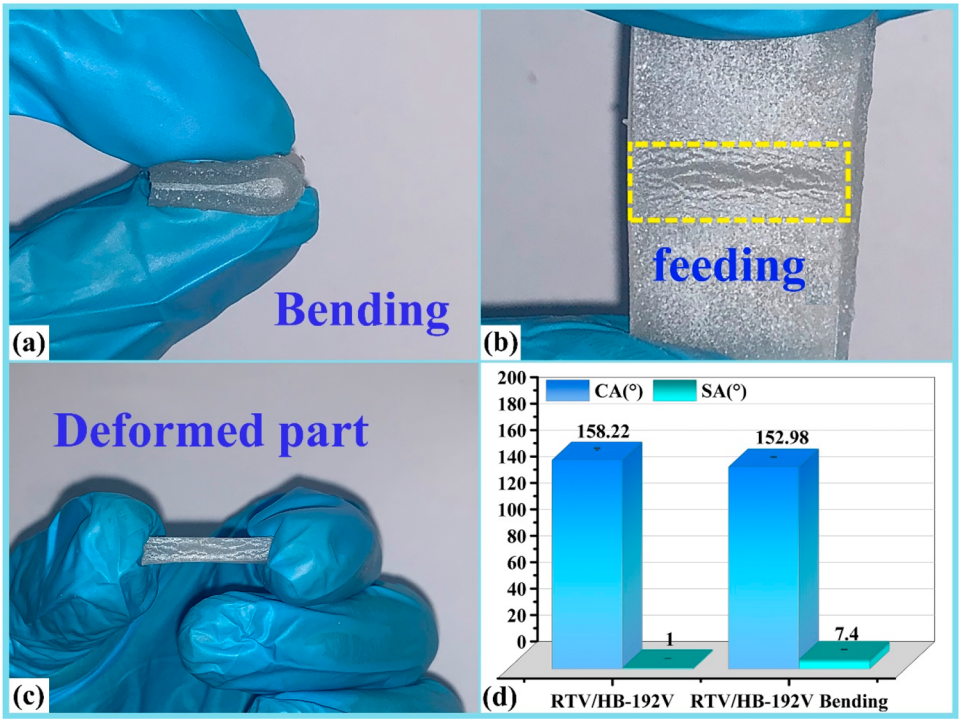

Figure 8. Bending test diagram of RTV/HB-192V (a−c) and comparison diagram of the contact angle and rolling angle of RTV/HB-192V before and after bending (d).

aging, the functional groups on the surfaces of RTV and RTV/HB-192V did not change obviously after 72 h of high-temperature aging.

Figure 8(a−c) was the test chart of RTV/HB-192V specimen bent 500 times, and Figure 8(c) was the most damaged part taken out from the bending test, which was used for a hydrophobic test. The test was repeated five times, and the measured data were counted. According to Figure 8(a−d), after the RTV/HB-192V was bent 500 times, the contact angle of the bent part measured by the contact angle tester was 152.98 ± 0.72°, and the rolling angle was 7.4 ± 0.62°, which was 5.24° lower than that of the original RTV/HB-192V. The rolling angle was 6.40° higher. According to the analysis of Figure 8(c), the bending test caused the uneven dispersion of HB-192V particles on the surface of RTV/HB-192V, and some points exposed the surface of RTV. However, after 500 bending tests, the surface of RTV/HB-192V was still a superhydrophobic surface, which proved that the prepared superhydrophobic surface had good bending durability.

4. CONCLUSION

In this paper, the superhydrophobic surface was successfully prepared by covering a layer of HB-192V particles on the surface of liquid silicone rubber by a powder pressing method. This work had the characteristics of simple operation, high speed, low cost, and no environmental pollution. The self-cleaning test, normal temperature drop bounce test, high-temperature aging test, and antibending durability test had been carried out, and some main conclusions were as follows.

(1) The RTV/HB-192V superhydrophobic surface prepared by the powder pressing method was green and pollution-free, which can form a superhydrophobic layer quickly and at low cost. It also had good self-cleaning, high-temperature resistance, and good bounce performance in a normal temperature drop bounce test.

(2) By covering a layer of HB-192V particles on the surface of liquid silicone rubber to make a microstructure, the contact angle of the rubber surface was increased from 112.84 ± 0.55° to 158.22 ± 2.01°, and the rolling angle was decreased from 51.02 ± 0.78° to 1.00 ± 0.50°.

(3) After 500 antibending tests, the contact angle of the prepared superhydrophobic surface was 152.98 ± 0.72°, and the rolling angle was 7.40 ± 0.62°, which proves that the prepared superhydrophobic surface had good antibending durability.

AUTHOR INFORMATION

Corresponding Authors

Qiang He − *College of Mechanical and Electrical Engineering, Gansu Agricultural University, Lanzhou 730070, China; College of Civil Aviation Safety Engineering, Civil Aviation Flight University of China, Sichuan, Guanghan 618307, China; Henan Joint International Research Laboratory of Man Machine Environment and Emergency Management, Henan, Anyang 455000, China;* orcid.org/0000-0003-4948-7887; Email: aystar@163.com

Fei Dai − *College of Mechanical and Electrical Engineering, Gansu Agricultural University, Lanzhou 730070, China;* Email: daifei@gsau.edu.cn

Authors

Zhen Wei − *College of Mechanical and Electrical Engineering, Gansu Agricultural University, Lanzhou 730070, China; College of Civil Aviation Safety Engineering, Civil Aviation Flight University of China, Sichuan, Guanghan 618307, China; Henan Joint International Research Laboratory of Man*

https://doi.org/10.1021/acsomega.2c07241
ACS Omega 2023, 8, 8548−8556

Machine Environment and Emergency Management, Henan, Anyang 455000, China

Fangyuan Zhang − *College of Mechanical and Electrical Engineering, Gansu Agricultural University, Lanzhou 730070, China; College of Civil Aviation Safety Engineering, Civil Aviation Flight University of China, Sichuan, Guanghan 618307, China; Henan Joint International Research Laboratory of Man Machine Environment and Emergency Management, Henan, Anyang 455000, China*

Complete contact information is available at: https://pubs.acs.org/10.1021/acsomega.2c07241

Notes

The authors declare no competing financial interest.

■ ACKNOWLEDGMENTS

This research project was supported by Sichuan Science and Technology Plan Project (23NSFSC1923).

■ REFERENCES

(1) Liu, F.; Du, H.; Han, Y.; Wang, C.; Liu, Z.; Wang, H. Recent Progress in the Fabrication and Characteristics of Self-Repairing Superhydrophobic Surfaces. *Adv Mater Interfaces* **2021**, *8* (17), 2100228.

(2) Li, A.; Zhao, Y.; Ren, S.; Zhang, F.; Zhang, F.; He, Q. Preparation and Comprehensive Performance Test of Superhydrophobic Paper Mulch Films. *ACS Omega* **2021**, *6* (38), 24407−24418.

(3) Wei, X.; Cao, X.; Yin, P.; Ding, Q.; Lu, Z.; Zhang, G. Design of a novel superhydrophobic F&Si-DLC film on the internal surface of 304SS pipes. *Diam Relat Mater* **2022**, *123*, 108852.

(4) Chen, X.; Wang, P.; Zhang, D.; Ou, J. Rational fabrication of superhydrophobic surfaces with coalescence-induced droplet jumping behavior for atmospheric corrosion protection. *Chem Eng J* **2022**, *428*, 132029.

(5) Kuang, Y.; Jiang, F.; Zhu, T.; Wu, H.; Yang, X.; Li, S.; Hu, C. One-step electrodeposition of superhydrophobic copper coating from ionic liquid. *Mater Lett* **2021**, *303*, 130579.

(6) Kong, Y.; Zhang, S.; Gao, Y.; et al. Low-temperature carbonization synthesis of carbon-based super-hydrophobic foam for efficient multi-state oil/water separation. *J Hazard Mater* **2022**, *423*, 127064.

(7) Gao, Y.; Xu, Y.; Zeng, W.; Fang, Z.; Duan, K.; Pei, G.; Zhou, W. Salt-frost resistance and mechanism analysis of super-hydrophobic pavement cement concrete for different deicing salts. *Road Mater Pavement* **2021**, *22* (8), 1908−1929.

(8) Kaewsaneha, C.; Roeurn, B.; Apiboon, C.; Opaprakasit, M.; Sreearunothai, P.; Opaprakasit, P. Preparation of Water-Based Alkyl Ketene Dimer (AKD) Nanoparticles and Their Use in Super-hydrophobic Treatments of Value-Added Teakwood Products. *ACS Omega* **2022**, *7* (31), 27400−27409.

(9) Ruzi, M.; Celik, N.; Onses, M S. Superhydrophobic coatings for food packaging applications: A review. *Food Packaging Shelf* **2022**, *32*, 100823.

(10) Ma, L.; Wang, J.; Zhang, Z.; Kang, Y.; Sun, M.; Ma, L. Preparation of a superhydrophobic TiN/PTFE composite film toward self-cleaning and corrosion protection applications. *J Mater Sci* **2021**, *56* (2), 1413−1425.

(11) Yu, X.; Shi, X.; Xue, F.; Bai, W.; Li, Y.; Liu, Y.; Feng, F. SiO_2 nanoparticle-containing superhydrophobic materials with enhanced durability via facile and scalable spray method. *Colloid Surface A* **2021**, *626*, 127014.

(12) Lei, S.; Fang, X.; Ou, J.; Wang, F.; Xue, M.; Li, W.; Amirfazli, A.; Chini, S. F. Icing of static and high-speed water droplets on superhydrophobic surface. *Mater. Lett.* **2021**, *285*, 129048.

(13) Ellis-Terrell, C.; Wei, R.; McKnight, R.; Huang, X.; Lin, K. Thermal stability of superhydrophobic and oleophobic silica nano-particle spray coating. *Mater Today Commun* **2020**, *25*, 101370.

(14) Yang, R.; Zuo, S.; Song, B.; Mao, H.; Huang, Z.; Wu, Y.; Cai, L.; Ge, S.; Lian, H.; Xia, C. Hollow Mesoporous Microspheres Coating for Super-Hydrophobicity Wood with High Thermostability and Abrasion Performance. *Polymers-Basel* **2020**, *12* (12), 2856.

(15) Sharma, D.; Kumar, R.; Avasthi, D.; Sikarwar, B. Self Assembly of Super-Hydrophobic Nanotextured Methyl Functionalized Silica on Copper and Aluminium Surfaces for Moist Air Condensation. *Colloid Surface A* **2020**, *605*, 125379.

(16) Daneshmand, H.; Sazgar, A.; Araghchi, M. Fabrication of robust and versatile superhydrophobic coating by two-step spray method: An experimental and molecular dynamics simulation study. *Appl Surf Sci* **2021**, *567*, 150825.

(17) He, Q.; Xu, Z.; Li, A.; Wang, J.; Zhang, J.; Zhang, Y. Study on hydrophobic properties of fluororubber prepared by template method under high temperature conditions. *Colloid Surface A* **2021**, *612*, 125837.

(18) Zhao, Y.; Peng, C.; Cui, S.; Wu, X.; Jiang, S. Microstructure Characterization and Oil Absorption Performance of Superhydrophobic Cotton Cellulose Aerogel. *J Wuhan Univ Technol* **2021**, *36* (4), 538−545.

(19) Luo, X.; Weng, Y.; Wang, S.; Du, J.; Wang, H.; Xu, C. Superhydrophobic and oleophobic textiles with hierarchical micro-nano structure constructed by sol-gel method. *J Sol-Gel Sci Techn* **2019**, *89* (3), 820−829.

(20) Wei, D.; Wang, J.; Liu, Y.; Wang, D.; Li, S.; Wang, H. Controllable superhydrophobic surfaces with tunable adhesion on Mg alloys by a simple etching method and its corrosion inhibition performance. *Chem Eng J* **2021**, *404*, 126444.

(21) Bangi, U.; Ransing, A.; Lee, K.; Park, H. Self-cleaned zirconia coatings prepared using a co-precursor sol-gel method. *Surf Eng* **2021**, *37* (8), 1059−1066.

(22) Chi, F.; Liu, D.; Wu, H.; Lei, J. Mechanically robust and self-cleaning antireflection coatings from nanoscale binding of hydrophobic silica nanoparticles. *Sol Energ Mat Sol C* **2019**, *200*, 109939.

(23) Wang, Y.; Yan, P.; Huo, X.; Liu, M.; Zhang, H.; Jiang, Z. 3D network super-hydrophobic hexafluorbisphenol A poly (aryl ether ketone) membrane prepared by one-step electrospraying. *High Perform Polym* **2020**, *32* (10), 1094−1101.

(24) He, S.; Zhan, Y.; Zhao, S.; Lin, L.; Hu, J.; Zhang, G.; Zhou, M. Design of stable super-hydrophobic/super-oleophilic 3D carbon fiber felt decorated with Fe_3O_4 nanoparticles: Facial strategy, magnetic drive and continuous oil/water separation in harsh environments. *Appl Surf Sci* **2019**, *494*, 1072−1082.

(25) Davis, A.; Surdo, S.; Caputo, G.; Bayer, I.; Athanassiou, A. Environmentally benign production of stretchable and robust super-hydrophobic silicone monoliths. *ACS Appl Mater Inter* **2018**, *10* (3), 2907−2917.

(26) Bayer, I. Superhydrophobic coatings from ecofriendly materials and processes: a review. *Adv Mater Interfaces* **2020**, *7* (13), 2000095.

(27) Qu, T.; Liu, R.; Dong, Y.; Ke, Y.; Yao, X. Experimental study on dynamic friction performances of rubber seals for aircraft doors. *Engineering Mechanics* **2020**, *37* (07), 247−256.

(28) Zhan, Y.; He, S.; Hu, J.; Zhao, S.; Zeng, G.; Zhou, M.; Zhang, G.; Senguptae, A. Robust super-hydrophobic/super-oleophilic sandwich-like UIO-66-F_4@rGO composites for efficient and multitasking oil/water separation applications. *J Hazard Mater* **2020**, *388*, 121752.

(29) Khaskhoussi, A.; Calabrese, L.; Proverbio, E. Superhydrophobic self-assembled silane monolayers on hierarchical 6082 aluminum alloy for anti-corrosion applications. *Applied Sciences* **2020**, *10* (8), 2656.

(30) Wang, G.; Li, A.; Zhao, W.; Xu, Z.; Ma, Y.; Zhang, F.; Zhang, Y.; Zhou, J.; He, Q. A review on fabrication methods and research progress of superhydrophobic silicone rubber materials. *Adv. Mater. Interfaces* **2021**, *8* (1), 2001460.

(31) Wang, G.; Li, A.; Li, K.; Zhao, Y.; Ma, Y.; He, Q. A fluorine-free superhydrophobic silicone rubber surface has excellent self-cleaning and bouncing properties. *J Colloid Interf Sci* **2021**, *588*, 175−183.

(32) Maghsoudi, K.; Momen, G.; Jafari, R.; Farzaneh, M. Direct replication of micro-nanostructures in the fabrication of super-

hydrophobic silicone rubber surfaces by compression molding. *Appl Surf Sci* **2018**, *458*, 619−628.
(33) Wan, Z.; Liu, Y.; Chen, S.; Song, K.; Peng, Y.; Zhao, N.; Ouyang, X.; Wang, X. Facile fabrication of a highly durable and flexible MoS_2@RTV sponge for efficient oil-water separation. *Colloid Surf. A* **2018**, *546*, 237−243.
(34) Wang, L.; Tian, Z.; Jiang, G.; Luo, X.; Chen, C.; Hu, X.; Zhang, H.; Zhong, M. Spontaneous dewetting transitions of droplets during icing & melting cycle. *Nat. Commun.* **2022**, *13* (1), 1−15.

https://doi.org/10.1021/acsomega.2c07241
ACS Omega 2023, 8, 8548−8556